NASA TECHNICAL
MEMORANDUM
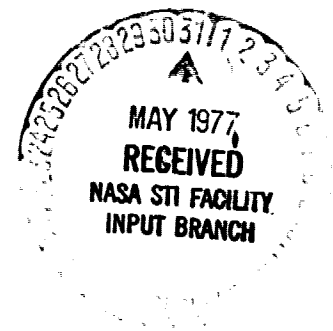
SPECTROSCOPIC DETERMINATION OF ELECTRICAL CONDUCTIVITY IN AN MHD DUCT FROM ABSOLUTE INTENSITY MEASUREMENTS

by S. Y. Wang and J. Marlin Smith
Lewis Research Center
Cleveland, Ohio 44135

SPECTROSCOPIC DETERMINATION OF ELECTRICAL CONDUCTIVITY
IN AN MHD DUCT FROM ABSOLUTE INTENSITY MEASUREMENTS

S. Y. Wang* and J. Marlin Smith
NASA Lewis Research Center
Cleveland, Ohio

I. Introduction

Measurements of the electrical conductivity in the NASA Lewis cesium seeded, H_2-O_2 MHD duct have been previously reported[1]. These measurements were performed in constant area, heat sink, cylindrical, Hall type MHD channels. The electrical conductivity was measured in the classical manner[2] by applying a voltage across the channel from one end electrode to the other, measuring the current, and using the inner electrodes as probes to monitor the voltage distribution along the channel. The average electrical conductivity was then determined from the relation

$$<\sigma> = \frac{I}{A(\Delta V/\Delta X)}$$

where: $<\sigma>$ is the electrical conductivity
   A is the cross sectional area of the
     channel
   I is the measured current
   $\Delta V/\Delta X$ is the voltage gradient determined
     from the linear portion of the voltage
     curve

These measurements were found to be in good agreement with theory except at low combustion pressures and/or high ratios of seed/oxygen mass flows (seed was injected into oxygen flow line). A possible explanation for these deviations was believed to be the result of poor atomization of the seed at high seed/oxygen mass flow ratios which resulted in droplet sizes which did not completely vaporize during their residence time in the combustor.

In order to corroborate the above measurements and to analyze the possibility of non-uniform seed injection as a cause of the above deviations, a spectroscopic investigation of the plasma conductivity has been undertaken. Transverse profiles of the absolute integrated intensity were measured from the optically thin lines of CSI-.5664 µ M and .5636 µ M. Radial profiles of emission coefficient were obtained from the measured transverse profiles of intensity by Abel inversion. Radial profiles of electrical conductivity were then obtained under two different assumptions. In the first the Cs seed fraction is assumed uniform and equal to the measured flow rate at the time when the temperature and conductivity were obtained. In the second method the local temperature and pressure are taken to be those given by a one-dimensional channel calculation including heat transfer and friction. In this case profiles of conductivity and seed fractions are obtained. The results of the two methods are compared to the previously measured[1] conductivity.

II. Experimental Apparatus and Procedure

The optical system is shown in fig. 1. General survey of the cesium atomic transition line spectrum in the visible region is done with both the spectrograph and the scanning monochromator. The monochromator has a 5x5 cm plane grating of 1200 grooves/mm, which provides a linear reversal dispersion of 1.6×10^{-9} M. Two optically-thin lines, CSI-.5664 µ M and .5636 µ M and a continuum at .5704 µ M (used as continuum correction for lines) were found appropriate for absolute intensity profile measurement[3].

Light from the plasma passing through the nitrogen-purged window is first directed by a stationary mirror onto a reversible rotating mirror. The rotating mirror is used to obtain the transverse scan of the plasma image which is passed through a lens and brought to focus at the entrance slit (30-60 µ m)of the monochromator. Using a PM tube, transverse profiles of the integrated intensities through the exit slit (600-1200 µ m) are recorded on a memory oscilloscope. Calibration is done for every optical path, using a 4x38 mm tungsten-ribbon filament lamp for reference behind the nitrogen-purged window.

III. Data Reduction

The data reduction procedure begins with the calibration curve[3]. A third order polynomial curve is least square fitted in terms of V_{PM} (the PM tube output voltage) Q_s (the radiant power flux per unit solid angle within a bandwidth $\Delta \lambda$) in the form:

$$Q_s = c_0 + c_1 V_{PM} + c_2 V_{PM}^2 + c_3 V_{PM}^3 \quad (1)$$

where Q_s is related to the Planck function Q_p (λ, T_t), the spectral emissivity of the tungsten filament $\epsilon(\lambda, T_t)$, and the transmittance of the lamp glass envelope $\tau(\lambda)$, as:

$$Q_s = \epsilon \tau Q_p \Delta \lambda \quad (2)$$

and the true temperature T_t of the tungsten filament is obtained from its brightness temperature, T_b, observed by a pyrometer of effective wavelength, λ_p, through Wien's law:

$$\frac{1}{T_t} = \frac{1}{T_b} + \frac{\lambda_p}{c_4} \ln \left[\tau \epsilon (\lambda_p, T_t) \right] \quad (3)$$

The transverse profiles of absolute integrated intensity are obtained from the recorded data of the PM tube output voltage of the traversing plasma image, using this calibration curve.

Data points (22) for the profile are divided into three zones and a least-square fit is made by a fourth degree polynominal as suggested by Cremers and Birkebak[4]. The transverse profiles of integrated intensity Q_y are next inverted to radial profiles of emission coefficient Q_r by Abel transformation shown below:

$$Q_y = 2 \int_0^{(R^2-y^2)^{1/2}} Q_r \, dZ = 2 \int_y^r \frac{Q_r \, r \, dr}{(r^2-y^2)^{1/2}} \quad (4)$$

and

*NRC Postdoctoral Research Fellow

1

$$Q_r = \frac{1}{-\pi} \int_r^R \frac{\frac{dQ_y}{dy}}{(y^2 - r^2)^{\frac{1}{2}}} \, dy \qquad (5)$$

Numerically the Nester-Olsen technique[5] is employed. Under the assumption of local thermodynamic equilibrium the measured radial profile of the emission coefficient, Q_r, can be related to the temperature and number density of neutral cesium atoms. The radiated power per unit volume, per unit solid angle, and per unit wavelength interval (watts/m^3-Sr-A) is[6]:

$$\epsilon = \frac{hc}{4\pi\lambda_0} \, L_\lambda \, A_{nm} \, N_m \qquad (6)$$

where L_λ is taken to be the normalized Lorentz profile

$$L_\lambda = \frac{W_{\frac{1}{2}}/\pi}{(\lambda_0 - \lambda)^2 + (W_{\frac{1}{2}})^2} \qquad (7)$$

for a line center at λ_0 with halfwidth $W_{\frac{1}{2}}$. A_{nm} is the transition probability between lower level n and upper level m. N_m is the number density at upper level m, related to the total number density (N_{sn}) of neutral cesium atoms by the Boltzmann relation:

$$N_m = N_{sn} \frac{g_m}{Z_s} \exp (-E_m/kT) \qquad (8)$$

where Z_s is the partition function of the cesium atom.

Relating the transition probability (A_{nm}) and the absorption oscillation strength (f_{mn}) by

$$A_{nm} = \frac{8\pi r_0 c}{\lambda_0^2} \frac{g_n}{g_m} f_{mn} \qquad (9)$$

the emission coefficient radiated over the bandwidth $\Delta\lambda$ of a spectral line is:

$$Q_r = \int_{\Delta\lambda} \epsilon \, d\lambda = \frac{hc}{4\pi\lambda_0} \frac{A_{nm} N_{sn} g_m F}{Z_s} \exp \left[\frac{E_m}{-kT}\right] (10)$$

$$\text{where} \quad F \equiv \frac{\int_{\Delta\lambda} \epsilon \, d\lambda}{\int_0^\infty \epsilon \, d\lambda} \qquad (11)$$

The function F is plotted in ref. 7 as a function of the volumetric absorption coefficient and the ratio of bandwidth to halfwidth, and is approximately equal to one for the present experiment. Values of the upper energy state (E_m), the statistical weight (g_m), and the transition probability (A_{nm}) are found in references 8 and 9.

Equation 10 relates the measured values of intensity, Q_r, to the local values of temperature and cesium neutral atom density. Two methods have been used to relate this experimentally measured intensity to the average electrical conductivity of the gas.

Method I - Constant Seed Fraction Method

In this method the seed is assumed to be uniformly distributed across the cross section of the channel. Then with measured values of hydrogen, oxygen, and seed flow rates as well as static pressure, the temperature and free electron density were determined as a function of radius from the measured values of Q_r (eq. 5), using a chemical equilibrium composition program[10]. The electrical conductivity at each point was then calculated as discussed in ref. 1.

Method II - Variable Seed Fraction Method

In this method the temperature and pressure at the point of the intensity measurement were determined from measured values of hydrogen and oxygen flow rates and combustion pressure using the chemistry of ref. 10 and taking into account a 3% heat loss in the combustor-nozzle and a 1% heat loss in the channel. The seed fraction was then adjusted until Q_r as calculated by equation 10 agreed with the measured value of Q_r as obtained from equation 5.

IV. Results and Discussion

In figure 2 the results of conductivity measurements obtained in reference 1 are shown for a combustion pressure of 1.034×10^6 N/M^2 (150 psia). It is seen that substantial agreement with theory is obtained up to a seed fraction of approximately .05 after which the conductivity falls below the theoretical curve. A possible explanation of this fall off was attributed in reference 1 to poor atomization and hence vaporization of seed at high seed to oxygen flow rates (seed was injected into oxygen line as a 75% solution of CSOH in water). It was the purpose of the present study to investigate this effect by more directly measuring the local plasma properties.

A typical temperature profile as obtained from the constant seed fraction method is shown in figure 3. It is seen that the profile is qualitatively what one might expect for a hot gas flowing in a cold wall channel (the channel walls in these experiments were copper heat sinked). The corresponding profile of electrical conductivity is shown in figure 4. The average electrical conductivity across the channel cross section was then obtained by integrating the conductivity profile over the cross section and dividing by the area.

$$\langle\sigma\rangle \equiv \frac{1}{A} \int \sigma \, dA \qquad (12)$$

Average values of conductivity for various seed fractions are shown in figure 5 for two different wavelengths. It is seen that the data are in substantial agreement with theory even at seed fractions well above the .05 cutoff observed in reference 1.

In figure 6 the average electrical conductivity as obtained under the assumption of a variable seed fraction method is shown as a function of seed fraction. Again there is substantial agreement with theory with no fall off of measured conductivity at seed fractions above .05. Comparison of figures 5 and 6 shows that the average conductivities obtained by the two methods discussed in this paper are substantially in agreement.

V. Concluding Remarks

The average conductivities as inferred from absolute intensity measurements of the optically thin lines of CsI-.5664 μM and .5636 μM have been shown to agree with theoretical calculations over the range of seed fractions investigated (.01 to .1). This differs from the conductivity cell measurements obtained in reference 1 in which, for seed fractions greater than .05, the measured conductivity began to fall progressively below the theoretical curve. No explanation for this discrepancy is presently known since both sets of data are consistently reproducible.

It should be noted however that conductivities could only be inferred by the present technique since equation 10 shows the measurement of the intensity does not uniquely define both the temperature and the cesium neutral particle density. Therefore, one or the other must be obtained by an independent measurement or inferred from theory. The latter method was used in this paper as discussed in the text. However, by measuring the intensity of two lines and ratioing their intensities the cesium neutral particle density drops out (see equation 10) and the temperature is uniquely determined by the intensity ratio. The particle density is then uniquely determinable from either of the line intensities. This was the original intent of the present work; however, run-to-run reproducibility was insufficient to employ the technique to any degree of accuracy and equipment was not immediately available to simultaneously measure the lines.

We are now measuring the conductivities at other combustion pressures and a two-dimensional computer code based on the Patankar-Spalding method[11] has been formulated to more accurately account for thermal boundary layers in interpreting the data.

References

1. Smith, J. M.: Results and Progress on the NASA Lewis H_2-O_2 MHD Program. 15th Symp. on the Engineering Aspects of Magnetohydrodynamics. The Univ. of Penn., Philadelphia, PA, May 24-26, 1976.

2. Heywood, J. B. and Womack, G. J., eds.: Open Cycle MHD Power Generation. Pergamon Press (London), 1969, p. 346.

3. Wang, S. Y.: Spectroscopic Measurement of a Seeded Combustion Plasma Jet. 18th Annual Meeting of the American Physical Society, Division of Plasma Physics, San Francisco, CA,

November 15-19, 1976.

4. Cremers, C. J. and Berkebak, R. C.: Application of the Abel Integral Equation to Spectrographic Data. Applied Optics, Vol. 5, pp. 1057-1064, 1966.

5. Nester, O. H. and Olsen, H. N.: Numerical Methods for Reducing Line and Surface Probe Data. SIAM Review, Vol. 2, No. 3, pp. 200-207, 1960.

6. Griem, H. R.: Plasma Spectroscopy. McGraw-Hill, 1964.

7. Morris, J. C.; Krey, R. V.; and Garrison, R. L.: Radiation Studies of Arc Heated Nitrogen, Oxygen, and Argon Plasmas. ARL 68-0103, 1968.

8. Agnew, L. and Summers, C.: Quantitative Spectroscopy of Cesium Plasma, Proceedings of the VII International Conference on Phenomena in Ionized Gases. Belgrad, Vol. II, 1966.

9. Atomic Energy Levels. NSRDS-NBS 35, Vol. III, 1971.

10. Gordon, S. and McBride, B. J.: Computer Program for Calculations of Complex Chemical Equilibrium Compositions, Rocket Performance, Incident and Reflected Shocks, and Chapman-Jouquet Detonations. NASA SP-273, 1967.

11. Patankar, S. V. and Spalding, D. B.: Heat and Mass Transfer in Boundary Layers, 2nd ed., 1970.

Symbols

A	cross section area of channel
A_{nm}	transition probability from nth to mth level
c	speed of light
c_0, c_1, c_2, c_3	defined by eq. 1
c_4	1.44×10^{-2} (m-k)
E_m	energy of the mth level
f_{mn}	absorption oscillation strength
g_m, g_n	statistical weight of upper and lower state
h	Planck's constant
I	electric current
k	Boltzmann's constant
L_λ	defined by eq. 7
N_m	number density of Cs atoms at the mth level
N_{sn}	number density of neutral Cs atoms
Q_p	Planck function
Q_r	emission coefficient
Q_s	defined by eq. 1
Q	integrated intensity
R	radius
r_0	classical radius of electron
S_f	mole fraction of neutral Cs atoms
T	gas temperature
T_b	brightness temperature
T_t	true temperature
$\Delta V / \Delta X$	voltage gradient
V_{pm}	PM tube voltage output
W	half halfwidth of spectral line

y	axis perpendicular to x
Z_s	partition function of Cs atom (=2)
ϵ	spectral emissivity
λ	wavelength
λ_o	wavelength at line center
λ_p	effective wavelength of pyrometer
$\Delta\lambda$	bandwidth
τ	transmittance
σ	local electrical conductivity
$\langle\sigma\rangle$	average electrical conductivity as defined by equation 12
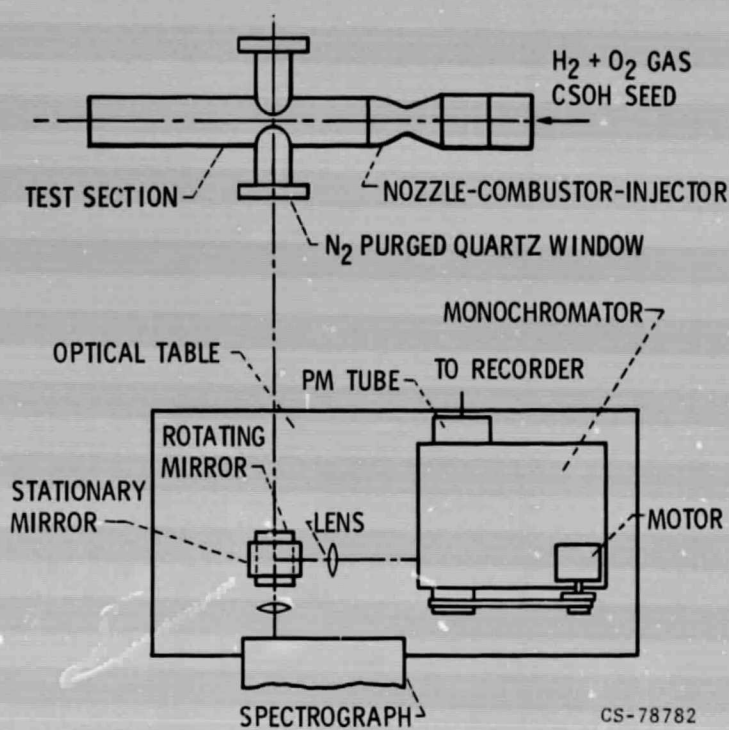
Figure 1. - Orientation of spectrographic equipment.
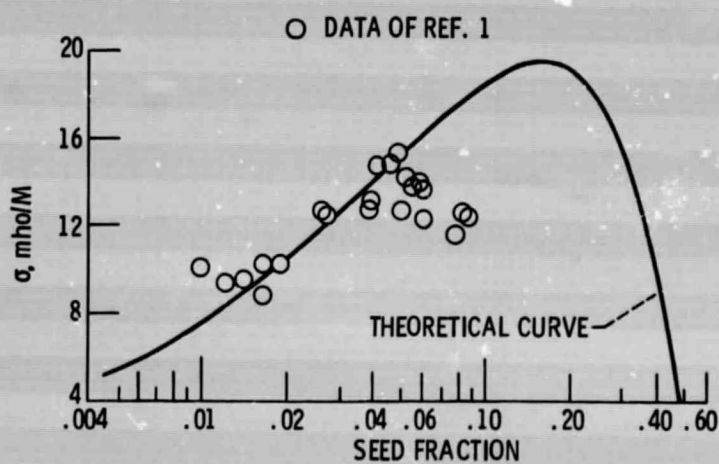
Figure 2. - Electrical conductivity versus seed fraction at a combustion pressure of 1.034×10^6 N/m^2 (150 psia).
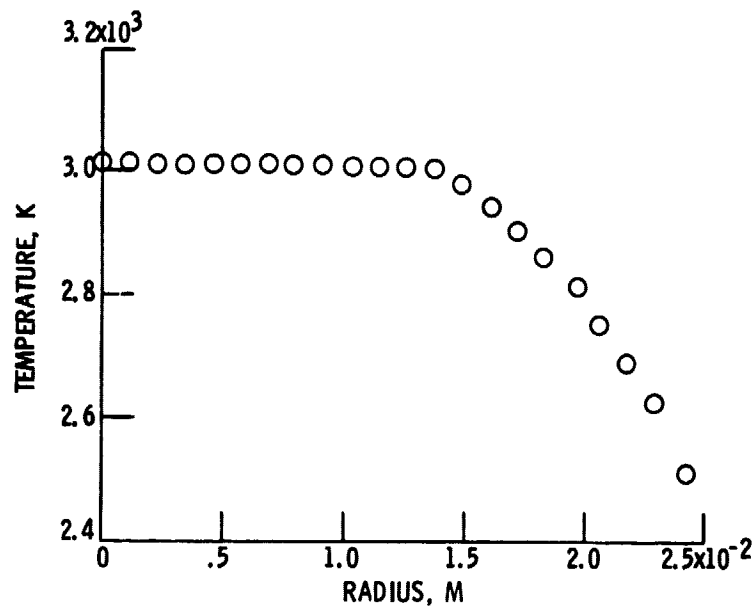
E-9118

CS-78782

Figure 3. - Radial profile of gas temperature determined from $C_S I - 0.5636 \, N/m^2$ (150 psia) and seed fraction of 1.4 percent.

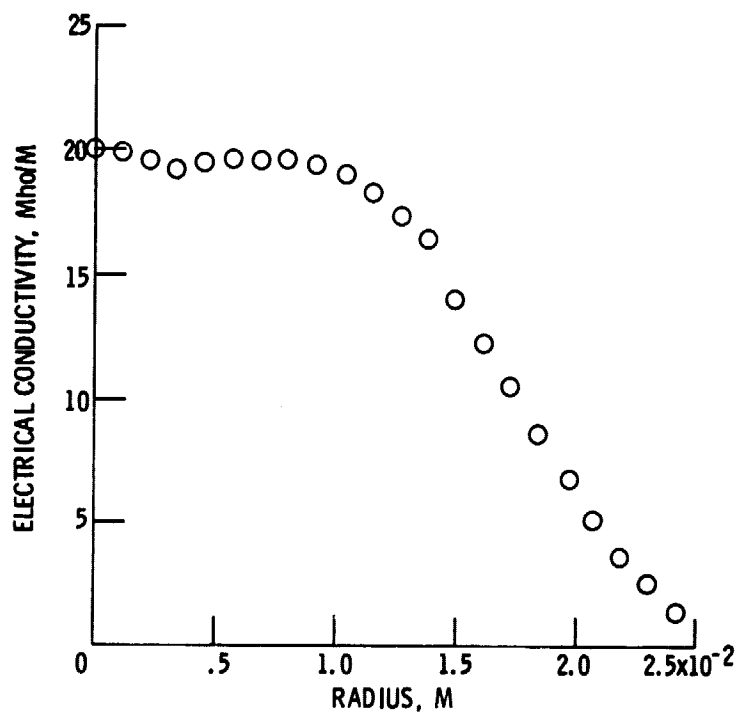Figure 4. - Radial profile of electrical conductivity determined from $C_S I - 0.5636 \, \mu M$ at chamber pressure of $1.034 \times 10^6 \, N/m^2$ (150 psia) and seed fraction of 1.4 percent.
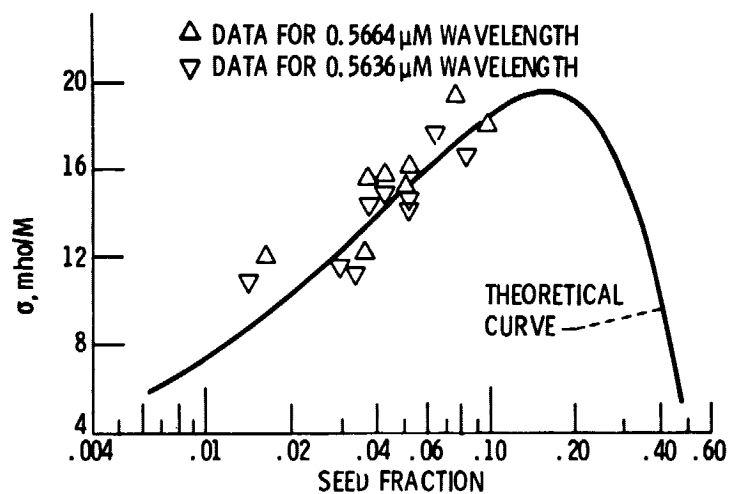
Figure 5. - Electrical conductivity versus seed fraction at
a combustion pressure of 1.034×10^6 N/m^2 (150 psia)
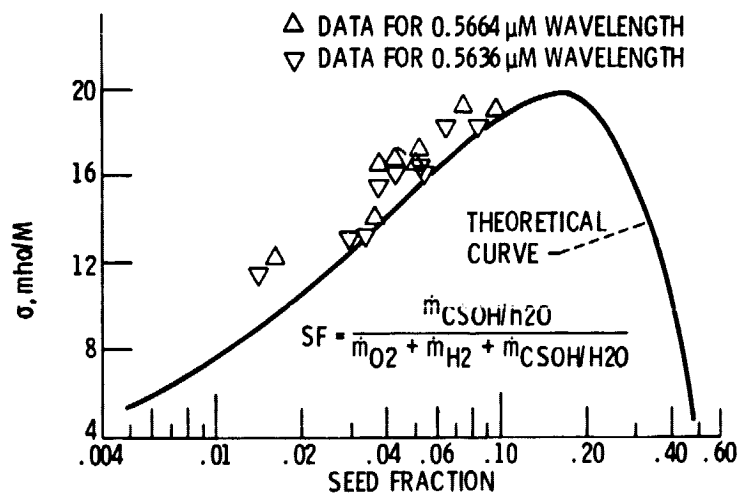constant seed fraction method.

Figure 6. - Electrical conductivity versus seed fraction at
a combustion pressure of 1.034×10^6 N/m^2 (150 psia)
variable seed fraction method.